J|A|C|S COMMUNICATIONS

Published on Web 08/24/2010

Aggregation Control of Hydrophilic Maghemite (γ-Fe_2O_3) Nanoparticles by Surface Doping Using Cerium Atoms

Amit H. Haviv,[†] Jean-Marc Grenèche,[‡] and Jean-Paul Lellouche*,[†]

Nanomaterials Research Center, Institute for Nanotechnology and Advanced Materials, Bar-Ilan University, Ramat-Gan 52900, Israel, and Laboratoire de Physique de l'Etat Condensé UMR CNRS 6087, Université du Maine, Le Mans 72085, France

Received April 19, 2010; E-mail: lellouj@mail.biu.ac.il

Abstract: The high-power ultrasonic irradiation of preformed magnetite (Fe_3O_4) nanoparticles in the presence of monoelectronic Ce-containing ceric ammonium nitrate [$Ce^{IV}(NH_4)_2(NO_3)_6$] oxidant in MeCOMe afforded hydrophilic 50 nm-sized colloidal, highly stable maghemite (γ-Fe_2O_3) nanoparticles. An "*inorganic*" Ce atom doping of the NP surface has been proposed in order to rationalize the observed nanoparticle antiaggregation phenomenon. Quite importantly, this method did not require the use of any organic ligand and/or polymer for the passivation of the nanoparticle surface.

The preparation of magnetic magnetite (Fe_3O_4) and maghemite (γ-Fe_2O_3) iron oxide nanoparticles (NPs) has been intensively examined for numerous applications such as magnetic storage,[1,2] biosensing applications,[3,4] magnetic separation,[5,6] drug delivery,[7,8] cancer hyperthermia,[9,10] and magnetic resonance imaging.[7,11,12] In this application-driven context, NP stabilization against detrimental aggregation is a critical parameter that needs to be controlled. Various NP capping methods based on charge- and/or steric-hindrance-mediated stabilization effects caused by polar capping species have been used for this purpose. These include *hydrophilic, water-compatible* citrate and tetramethylammonium (Me_4N^+) ions[13,14] and polymers [poly(ethylene glycol)s, polyacrylates, poly-L-lysine, diblock copolymers, polyols, and natural polysaccharides] or *hydrophobic* small ligands (oleyl amine/acid).[15] *Water-compatible* inorganic SiO_2 corona adlayers have also been readily deposited onto iron oxide NPs, enabling further functionalization.[16,17] Nevertheless, all of these passivation methods present specific limitations, including, for example, the following: (a) nanoparticulate compatibility toward either *organic* nonaqueous or *aqueous* physiological media; (b) NP size increase, which can detrimentally affect their mode of administration (i.e., infusion) and tissue compartmentalization/cellular uptake; (c) the expected reduction of NP neat magnetization; and (d) potential issues of biocompatibility and/or immunogenicity of passivating corona shells.[15]

Herein, the present study discloses novel experimental conditions leading to *hydrophilic water-compatible* maghemite (γ-Fe_2O_3) NPs with control of the NP aggregation level. The most remarkable fact concerning the NP aggregation control is that *these conditions involve neither any surface-passivating bifunctional ligand nor any routinely used physically adsorbed natural/non-natural polymer*. More specifically, the conditions comprise the high-power ultrasonic irradiation of preformed 10−15 nm-sized magnetite (Fe_3O_4) NPs in contact with ceric ammonium nitrate [CAN, $Ce^{IV}(NH_4)_2(NO_3)_6$]

Scheme 1. Fabrication of CAN-Stabilized Maghemite NPs

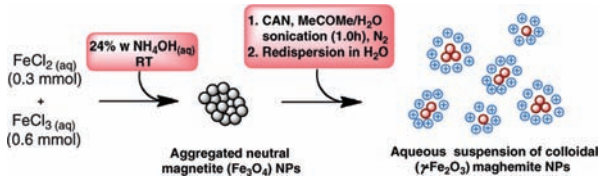

in a 1/1 v/v MeCOMe/H_2O mixture. CAN is a very strong monoelectronic oxidant that can oxidize numerous organic groups (e.g., alcohols/phenols, ethers/sulfides, enol ethers, and alkenes/polyenes).[18−20] It also promotes both oxidative radical-mediated formation and cleavage of carbon−carbon bonds.

In this way, the simultaneous oxidation of magnetite NPs to maghemite NPs[21,22] and CAN-mediated modification(s) of the NP surface charge/functionality (see below) resulted in crystalline, *hydrophilic*, strongly positively charged CAN-stabilized maghemite NPs that formed extremely stable colloidal water dispersions.

CAN-stabilized maghemite NPs were fabricated in two consecutive steps. The first involved the Massart-based fabrication of 10−15 nm-sized, *neutral*, brilliant black, freely flowing magnetite NPs via NH_4OH-mediated basic cohydrolysis of Fe^{2+}/Fe^{3+} iron salts (Scheme 1 and section SI-1a in the Supporting Information).[23] In the second step, the resulting neutral, black magnetite NPs were immediately suspended in a 1/1 v/v MeCOMe/H_2O solution of the CAN oxidant (0.01 mmol of CAN/mL of MeCOMe) and ultrasonicated (Sonics & Materials Vibra-Cell ultrasonic processor, titanium horn, 1 h; the optimized protocol is available in section SI-1b) to afford CAN-stabilized brown-colored maghemite NPs.

Transmission electron microscopy (TEM) microphotographs (JEOL-JEM 2010 microscope, 200 kV acceleration voltage, Formvar carbon 400 mesh grids; see section SI-2) of the starting magnetite NPs (Figure 1A) and CAN-stabilized maghemite NPs (Figure 1B,C) showed that the *neutral* 10−15 nm-sized magnetite NPs were highly aggregated. In contrast, the CAN-stabilized NPs appeared as loose ∼50/60 nm-sized clusters. The elementary CAN-stabilized NPs possessed a slightly anisotropic morphology with the same 10−15 nm average NP diameter as the starting magnetite NPs. In agreement with the TEM results, the average hydrodynamic diameter of the CAN-stabilized maghemite NPs was measured to be 50.0 nm using dynamic light scattering (DLS) [Malvern Nano-ZS Zetasizer/633 nm He−Ne laser, doubly distilled H_2O (ddH_2O)] with a polydispersity index of 0.18 (Figure 2, top left).

This value was indicative of the clustering of *three* to *five* 10−15 nm-sized elementary CAN-stabilized maghemite NPs. This result might be rationalized on the basis of the related *irreversible ultrasound-stable* clustering of intermediate preformed neutral Massart magnetite NPs (the first step of the two-step CAN-mediated process cited above; Scheme 1).

[†] Bar-Ilan University.
[‡] Université du Maine.

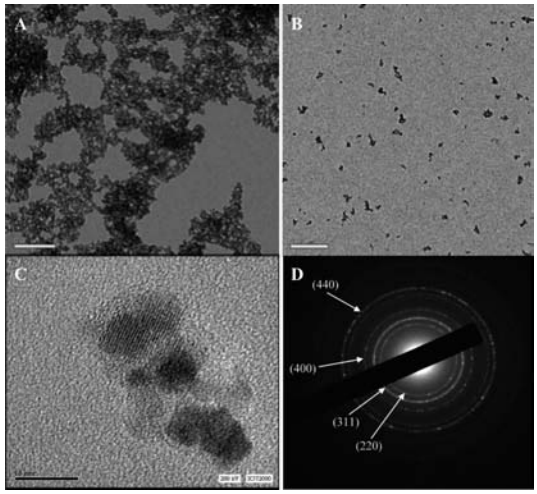

Figure 1. TEM images of (A) aggregated neutral magnetite NPs (low-resolution; scale bar represents 200 nm) and (B, C) CAN-stabilized maghemite NPs [high-resolution; scale bars represent (B) 200 and (C) 10 nm]. (D) SAED pattern.

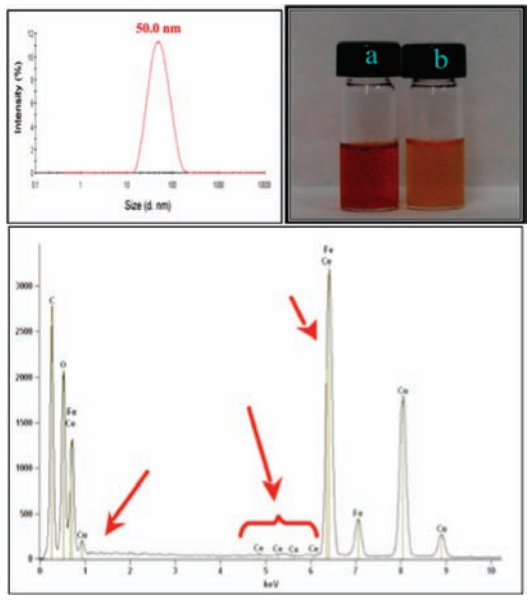

Figure 2. (top left) DLS curve and (bottom) compositional EDS elemental analysis of CAN-stabilized maghemite NPs (ddH_2O; red arrows indicate Ce-related peaks). (top right) Analytical colorimetric test for CAN-stabilized maghemite NPs in the presence (a) and absence (b) of Fe^{2+} cations.

Particle crystallinity was evidenced by the observation of lattice fringes using high-resolution TEM (Figure 1C) as well as by lattice imaging of the four indicated individual (220), (311), (400), and (440) diffraction planes obtained by selected-area electron diffraction (SAED) (Figure 1D) and powder X-ray diffraction (XRD) (maghemite spinel structure, JCPDS card no. 39-1346; Figure SI-4). These results emphasized that no fundamental structure change (potentially caused by Ce atom inclusion) occurred in the CAN−maghemite phase. However, since XRD was unable to unambiguously distinguish between *magnetite* (Fe_3O_4) and *maghemite* (γ-Fe_2O_3) phases, an additional sensitive colorimetric test based on the specific detection of ferrous Fe^{2+} versus ferric Fe^{3+} ions in acid-dissolved NP samples was performed.[24−26] This test exploits the capability of the strongly complexing bidentate 1,10-phenanthroline (*o*-phen) ligand to form the deep-red-colored ferroin complex $[Fe(o\text{-phen})_3]^{2+}$ with Fe^{2+} ions. Acid-digested magnetite and CAN-stabilized maghemite NP samples (2.0 mg, 0.1 M HCl) were separately treated with excess *o*-phen (1.0 M EtOH solution, 2.0 mL). The expected red color characteristic of Fe^{2+} developed only for the starting magnetite NP sample (Figure 2, top right, solution a). In contrast, the CAN−maghemite NP solution afforded a yellowish phase (Figure 2, top right, solution b), thus confirming the maghemite nature of the CAN-stabilized maghemite NPs.

A 9.0−9.5 nm average NP size for the CAN-stabilized maghemite NPs was determined using the Scherrer equation (XRD analysis), correlating well with the TEM and DLS analyses. Moreover, ^{57}Fe Mössbauer spectroscopy performed at 300 K afforded a spectrum disclosing asymmetrical sextets of broadened lines that were attributed to significant superparamagnetic fluctuations (Figure SI-9 bottom). In contrast, the corresponding lower-temperature 77 K spectrum (Figure SI-9 top) exhibited a similar but well-resolved sextet pattern. The mean isomer shift values were measured to be in the 0.42−46 and 0.35−0.37 mm/s ranges for the 77 and 300 K spectra, respectively.[27] These values were unambiguously assigned to tetra- and octahedrally coordinated Fe^{3+} ions. Such local electron density probe parameters allowed the presence of Fe^{2+} species to be excluded, in agreement with a maghemite phase.[27] These data confirmed the above-mentioned results of the *o*-phen colorimetric test. Interestingly, despite the fact that oxidative *magnetite* to *maghemite* phase transformations are known,[28] the present ultrasound-assisted CAN-mediated oxidation of magnetite to maghemite NPs has no precedent.

NP surface effects potentially introduced by this oxidative process were further investigated using ζ-potential measurements (Figure SI-3a). Quite strongly positive values in the range +40.0 to +43.0 mV range were obtained, depending on the NP batch (aqueous solutions of NPs, 0.5 mg of NPs/mL of ddH_2O, pH 4.08; see section SI-2). The fact that these values were much higher than the commonly accepted border value of +25.0 mV indicated that the remarkably high colloidal stability of CAN-stabilized γ-Fe_2O_3 NPs was due to repulsive interactions between the strongly positively charged NPs. Moreover, such a charge-mediated property of NPs (ζ potential > +25 mV) was also preserved in the 4.0−7.5 pH range (Figure SI-3b), as measured by NP basic titration/neutralization using 0.1 M NaOH (aqueous solution of NPs, 0.5 mg NPs/mL ddH_2O, Malvern MPT-2 autotitrator). Therefore, the combined XRD and ζ-potential analyses suggested that the magnetite to maghemite phase transformation rather affected the surface/surface charge properties of the resulting NPs. Confirmation emerged from both energy-dispersive X-ray spectroscopy (EDS) and surface-sensitive X-ray photoelectron spectroscopy (XPS) analyses. Indeed, EDS analysis led to a low-level detection of Ce (0.24 wt %, 0.02 atom %; Figure 2 bottom and Table SI-5), indicative of *NP surface doping by Ce atoms* to produce highly stable colloidal water suspensions of NPs. Second, the potential CAN-based surface modification of CAN-stabilized maghemite NPs was also investigated using XPS. One broad peak appeared at a binding energy (BE) in the 880−914 eV range that was ascribed to Ce 3d electrons (Figure SI-6). Interestingly, the additional Fe $2p_{3/2}$ peak (BE = 710.8 eV) included one satellite peak at a BE of 719.0 eV, which is quite characteristic of a *maghemite* NP phase.

At this stage, the antiaggregation effect of the Ce-containing CAN oxidant had to be questioned for its specificity. For that purpose, two other oxidants *that do not contain cerium*, ammonium persulfate [APS, $(NH_4)_2S_2O_8$] and trimethylamine *N*-oxide (Me_3NO), were also tested for particle stabilization using the above-mentioned typical CAN protocol (sections SI-1 and SI-2). APS immediately afforded a substantial precipitation of strongly aggregated brown maghemite NPs (colorimetric *o*-phen test). In contrast, Me_3NO led to the formation of brown, water-compatible highly stabilized maghemite NPs. However, these NPs possessed an average diameter of 180.7 nm as measured by DLS (Figure SI-7 top), which is much bigger

Scheme 2. Ce Doping of the CAN-Stabilized Maghemite NP Surface

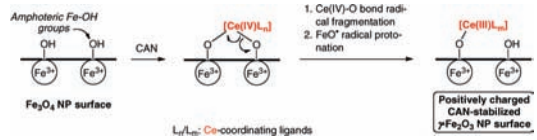

than that for the CAN-stabilized maghemite NPs. In addition, they disclosed a *negative* ζ potential (−39.1 mV; Figure SI-7 bottom), in contrast to the highly positive one observed for the CAN-stabilized maghemite NPs.

Thus, the antiaggregation effect of the Ce atom doping is quite unique and *specific to the CAN oxidant*. Although it is not fully clear, this intriguing effect has been tentatively rationalized according to Scheme 2. It was already known that Lewis acid−base interactions of surface magnetite Fe^{3+} atoms with H_2O molecules followed by H_2O ligand deprotonation can create interfacial amphoteric Fe−OH groups on the NP surface.[28,29] Under ultrasonic irradiation, CAN anions, $[Ce^{IV}(NO_3)_6]^{2-}$, might oxidatively react through (i) ligand-exchange of Ce-coordinated bidentate nitrato ligands and (ii) Ce^{IV}−O bond radical fragmentation/FeO$^{\bullet}$ radical protonation in order to attach multiply positively charged $Fe-O-Ce^{III}L_m$ complexes on the NP surface (where L is a Ce-coordinating ligand). Similar mechanistic considerations have been used to rationalize the oxidative radical-mediated CAN cyclization of 1,4/1,5-diols toward corresponding tetrahydropyran and tetrahydrofuran derivatives.[30]

For the sake of complete analysis, SQUID magnetization profiles of CAN-stabilized γ-Fe_2O_3 NPs and of the starting neutral magnetite NPs were obtained at 300 K. They showed the absence of any hysteresis loop, supporting NP superparamagnetism behavior (Figure SI-8). Under these conditions, the saturation magnetizations M_s were measured to be 59.48 and 73.54 emu/g with an observed blocking temperature of 151−152 K.

Finally, the potential cytotoxicity of CAN-stabilized γ-Fe_2O_3 NPs was also evaluated on HeLa, HEK 293, and MEF/3T3 cells using MTT assays (24 and 48 h incubations; section SI-10 and Figure SI-11). The MTT assays generally employed a cell-culture Dulbecco's minimum essential medium (DMEM) supplemented with 10% fetal calf serum and 1% antibiotics/glutamine (section SI-10). Therefore, protein adsorption onto the NP surface might likely result in NP aggregation and sedimentation near the surface of the cells, altering the NP−cell interactions and subsequent toxicity results. First and in this context, CAN-stabilized γ-Fe_2O_3 NPs (0.5 g/L in ddH_2O) were titrated using physiological DMEM (for protocol and titration curve details, see section SI-12). The particulate ζ potentials sharply decreased from +41.2 to +0.51 mV (section SI-12, table of data, entries 5 and 6), indicative of protein adsorption and NP aggregation. Second, the DMEM-mediated NP aggregation was tracked by DLS at various increasing concentrations of CAN-stabilized γ-Fe_2O_3 NPs (0.05, 0.1, 0.25, 0.5, and 0.75 g/L, 24 h incubation; Figure SI-13). The hydrodynamic diameters of the DMEM-driven NP aggregates slightly increased from 50.0 to 95.0−121.0 nm, confirming the role of DMEM in NP destabilization/aggregation. However, the aggregate diameters remained in the submicrometer range of 50−200 nm that is typically observed for particulate cell uptake.[31,32] Clearly, these last results validated the proposed MTT assay approach.

Therefore, in all of the MTT assays, the cell viability was not affected by the presence of the CAN−maghemite NPs, even at a high NP concentration of 1.0 g/L.[33] These data suggested that these novel Ce-modified maghemite NPs are highly biocompatible with further uses in vivo (e.g., MRI, drug delivery systems).

Acknowledgment. Funding by the VIth Framework European NACBO Project (NMP3-2004-500802-2) is acknowledged. Jonathan Lellouche and Prof. Aryeh Frimer are thanked for their help in MTT assays and English refinement, respectively.

Supporting Information Available: NP fabrication procedures and characterization/instrumentation, ζ-potential distribution curves, XRD/EDS and XPS analyses, DLS size distribution and ζ-potential characterizations of Me_3NO-stabilized maghemite NPs, magnetization profiles, 300/77 K ^{57}Fe Mössbauer spectra of CAN-stabilized γ-Fe_2O_3 NPs, cell-culturing protocol/MTT cytotoxicity tests, and NP aggregation graphs in DMEM obtained using DLS. This material is available free of charge via the Internet at http://pubs.acs.org.

References

(1) Sun, S.; Murray, C. B.; Weller, D.; Folks, L.; Moser, A. *Science* **2000**, *287*, 1989–1992.
(2) Guo, Q.; Teng, X.; Rahman, S.; Yang, H. *J. Am. Chem. Soc.* **2003**, *125*, 630–631.
(3) El-Boubbou, K.; Gruden, C.; Huang, X. *J. Am. Chem. Soc.* **2007**, *129*, 13392–13393.
(4) Liu, Z.; Wang, J.; Xie, D.; Chen, G. *Small* **2008**, *4*, 462–466.
(5) Hien Pham, T. T.; Cao, C.; Sim, S. J. *J. Magn. Magn. Mater.* **2008**, *320*, 2049–2055.
(6) Li, D.; Teoh, W. Y.; Selomulya, C.; Woodward, R. C.; Amal, R.; Rosche, B. *Chem. Mater.* **2006**, *18*, 6403–6413.
(7) Kim, J.; Lee, J. E.; Lee, S. H.; Yu, J. H.; Lee, J. H.; Park, T. G.; Hyeon, T. *Adv. Mater.* **2008**, *20*, 478–483.
(8) Rubio-Retama, J.; Zafeiropoulos, N. E.; Serafinelli, C.; Rojas-Reyna, R.; Voit, B.; Lopez Cabarcos, E.; Stamm, M. *Langmuir* **2007**, *23*, 10280–10285.
(9) Drake, P.; Cho, H.-J.; Shih, P.-S.; Kao, C.-H.; Lee, K.-F.; Kuo, C.-H.; Lin, X.-Z.; Lin, Y.-J. *J. Mater. Chem.* **2007**, *17*, 4914–4918.
(10) Kim, D.-H.; Kim, K.-N.; Kim, K.-M.; Lee, Y.-K. *J. Biomed. Mater. Res., Part A* **2009**, *88A*, 1–11.
(11) Brahler, M.; Georgieva, R.; Buske, N.; Muller, A.; Muller, S.; Pinkernelle, J.; Teichgraber, U.; Voigt, A.; Baumler, H. *Nano Lett.* **2006**, *6*, 2505–2509.
(12) Wan, J.; Cai, W.; Meng, X.; Liu, E. *Chem. Commun.* **2007**, 5004–5006.
(13) Liu, J.; Sun, Z.; Deng, Y.; Zou, Y.; Li, C.; Guo, X.; Xiong, L.; Gao, Y.; Li, F.; Zhao, D. *Angew. Chem., Int. Ed.* **2009**, *48*, 5875–5879.
(14) Vayssières, L.; Chanéac, C.; Tronc, E.; Jolivet, J. P. *J. Colloid Interface Sci.* **1998**, *205*, 205–212.
(15) Laurent, S.; Forge, D.; Port, M.; Roch, A.; Robic, C.; Vander Elst, L.; Muller, R. N. *Chem. Rev.* **2008**, *108*, 2064–2110.
(16) Philipse, A. P.; van Bruggen, M. P. B.; Pathmamanoharan, C. *Langmuir* **1994**, *10*, 92–99.
(17) Kim, J.; Kim, H. S.; Lee, N.; Kim, T.; Kim, H.; Yu, T.; Song, I. C.; Moon, W. K.; Hyeon, T. *Angew. Chem., Int. Ed.* **2008**, *47*, 8438–8441.
(18) Deleersnyder, K.; Schaltin, S.; Fransaer, J.; Binnemans, K.; Parac-Vogt, T. N. *Tetrahedron Lett.* **2009**, *50*, 4582–4586.
(19) Dhakshinamoorthy, A.; Pitchumani, K. *Catal. Commun.* **2009**, *10*, 872–878.
(20) Nuran, I.; Scedil, I. K.; Fatma, K.; Scedil, U.; Murat, I. *J. Appl. Polym. Sci.* **2009**, *114*, 40–48.
(21) Plaza, R. C.; Arias, J. L.; Espón, M.; Jiménez, M. L.; Delgado, A. V. *J. Colloid Interface Sci.* **2002**, *245*, 86–90.
(22) Sun, Y.-K.; Ma, M.; Zhang, Y.; Gu, N. *Colloids Surf., A* **2004**, *245*, 15–19.
(23) Massart, R.; Dubois, E.; Cabuil, V.; Hasmonay, E. *J. Magn. Magn. Mater.* **1995**, *149*, 1–5.
(24) Pyenson, H.; Tracy, P. H. *J. Dairy Sci.* **1945**, *28*, 401–412.
(25) McCullen, P. A. *J.—Assoc. Off. Anal. Chem.* **1978**, *61*, 968–970.
(26) Komadel, P.; Stucki, J. W. *Clays Clay Miner.* **1988**, *36*, 379–381.
(27) Daou, T. J.; Begin-Colin, S.; Grenèche, J. M.; Thomas, F.; Derory, A.; Bernhardt, P.; Legaré, P.; Pourroy, G. *Chem. Mater.* **2007**, *19*, 4494–4505.
(28) Schwertmann, U.; Cornell, R. M. *Iron Oxides in the Laboratory*, 2nd ed.; Wiley-VCH: Weinheim, Germany, 2000.
(29) Cheng, F.-Y.; Su, C.-H.; Yang, Y.-S.; Yeh, C.-S.; Tsai, C.-Y.; Wu, C.-L.; Wu, M.-T.; Shieh, D.-B. *Biomaterials* **2005**, *26*, 729–738.
(30) Alvarez-Manzaneda, E. J.; Chaboun, R.; Alvarez, E.; Cabrera, E.; Alvarez-Manzaneda, R.; Haidour, A.; Ramos, J. M. *Synlett* **2006**, 1829–1834.
(31) Mailänder, V.; Landfester, K. *Biomacromolecules* **2009**, *10*, 2379–2400.
(32) Safi, M.; Sarrouj, H.; Sandre, O.; Mignet, N.; Berret, J.-F. *Nanotechnology* **2010**, *21*, 145103.
(33) Improved cell viabilities were constantly observed for both HeLa and HEK 293 cells at 48 and 24 h, respectively. It is noteworthy that Ce^{III} cations have an ionic radius almost identical to that of bivalent Ca^{2+} ions (1.01 vs 1.0 Å, respectively). Accordingly, Ce^{III} salts are known to often interfere with numerous enzymatic processes/transformations, likely resulting in major biological/pharmacological effects. See the following reference for a recent overview of the subject: Jakupec, M. A.; Unfried, P.; Keppler, B. K. *Rev. Physiol. Biochem. Pharmacol.* **2005**, *153*, 101–111, As a matter of consequence, the observed improved cell viabilities may be envisaged as an indirect proof of the proposed surface doping of CAN-stabilized maghemite NPs by Ce^{III} atoms arising from CAN.

JA103283E